Fringe-free holographic measurements of large-amplitude vibrations

F. Joud,[1] F. Verpillat,[1] F. Laloë,[1] M. Atlan,[2] J. Hare,[1] and M. Gross[1,*]

[1]*Laboratoire Kastler-Brossel, UMR 8552 CNRS, École Normale Supérieure, Université Paris 6, 24 rue Lhomond 75231 Paris Cedex 05 France*

[2]*Institut Langevin, UMR 7587 CNRS INSERM, ESPCI ParisTech, Université Paris 6, Université Paris 7, 10 rue Vauquelin, 75 231 Paris Cedex 05, France*

**Corresponding author: gross@lkb.ens.fr*

Received August 19, 2009; accepted September 25, 2009;
posted October 21, 2009 (Doc. ID 115962); published November 24, 2009

In the measurement of the amplitude of vibration of objects, holographic imaging techniques usually involve fringe counting; because of the limited resolution of the images, measurements of large amplitudes are not accessible. We demonstrate a technique that suppresses the necessity of fringe counting—frequency sideband imaging—where the order of the sideband is considered a marker of the amplitude. The measurement is completely local: no comparison with another reference point on the object is necessary. It involves a sharp variation of a signal, which makes it robust against perturbations. The method is demonstrated in an experiment made with a vibrating clarinet reed; phase modulations as large as 1000 rad have been measured.

OCIS codes: 090.1760, 200.4880, 040.2840, 100.2000.

The observation of interference fringes in holographic methods provides accurate measurements of the amplitude of vibration of objects. Powell and Stetson [1] have shown that the fringes on the holographic reconstruction of a vibrating object correspond, after time averaging, to zeros of the Bessel function $J_0(\Phi)$, where $\Phi(x,y)$ is the amplitude of phase modulation of the optical field emitted by the object at point x,y. Digital holography was introduced in 1994 by Schnars and Jüptner [2]. In 2003 Picard *et al.* [3] transposed the time averaging method to digital holography.

In a previous Letter [4], we described sideband digital holography, based on the detection of the light backscattered by a vibrating object at different sideband frequencies; the fringes for sideband n then correspond to the zeros of the nth-order Bessel function $J_n(\Phi)$. As in the work by Aleksoff [5] in 1971, the reference beam was frequency shifted to select one sideband n, but the use of acousto-optic modulators and numerical techniques provided much more flexibility. In [4], we showed how the comparison of dark fringes for different sideband leads to a determination of the vibration amplitude $\Phi(x,y)$ at each point of the object. This determination is nonlocal, since it involves counting fringes from one reference point of the image to the point of interest, so that large amplitudes are not accessible.

In this Letter, we demonstrate another approach that completely eliminates the necessity of counting fringes; it gives a local measurement of the amplitude of vibration, even for large values. For any pixel of coordinate x,y, we consider the sideband order n a variable and we plot the intensity I as a function of n. One can then easily determine Φ, since $I(n)$ exhibits a sharp variation from maximum to zero near $n \simeq \Phi$. The method is robust and can easily be used even when the fringes become so narrow that they cannot be resolved, which gives immediate access to large amplitudes of vibration.

Consider a point of the object vibrating at frequency ν_A and amplitude $z_{\max}$; its displacement $z(t)$ is

$$z(t) = z_{\max} \sin(2\pi\nu_A t). \tag{1}$$

In backscattering geometry, this corresponds to a phase modulation:

$$\varphi(t) = 4\pi z(t)/\lambda = \Phi \sin(2\pi\nu_A t), \tag{2}$$

where λ is the optical wavelength and $\Phi = 4\pi z_{\max}/\lambda$. The scattered field is then

$$E(t) = \mathcal{E} e^{j(\nu_0 t + \varphi(t))} = \mathcal{E} \sum_n J_n(\Phi) e^{j(\nu_0 + n\nu_A)t}, \tag{3}$$

where $\mathcal{E}$ is the complex amplitude of the field, ν_0 is the frequency of the illumination optical field, and J_n is the nth-order Bessel function of the first kind; $J_{-n}(z) = (-1)^n J_n(z)$ for integer n and real z. The scattered field is then the sum of sidebands with frequencies $\nu_0 + n\nu_A$ and intensities I_n, given by

$$I_n(\Phi) = |\mathcal{E} J_n(\Phi)|^2. \tag{4}$$

Figure 1(a) shows the intensity of the sidebands as a function of n, assuming $\Phi = 30.3$ rad. When n is considered a continuous variable $n = (\nu - \nu_0)/\nu_A$ giving the Doppler frequency shift in units of ν_A, one obtains the light gray shade corresponding to the Doppler spectrum deduced from the vibration velocity distribution. This continuous spectrum is proportional to $[1-(n/\Phi)^2]^{-1/2}$, where n is confined between the values $\pm\Phi$ that correspond to the maximum Doppler shift. The discrete spectrum has a similar behavior, remaining mostly confined between the same n values and dropping abruptly from a maximum reached close to $n = \pm\Phi$ to almost zero. This is the key idea of our method: we measure the frequency position of this sharp variation and deduce from it the value of the vibration amplitude. This method can be seen as a discrete spectrum version of laser Doppler imaging of nonperiodic motions reported in [6,7].

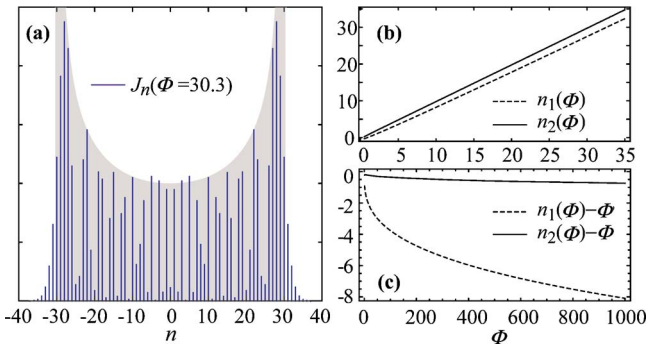

Fig. 1. (Color online) (a) Relative intensities of the sidebands as a function of n for fixed $\Phi=30.3$ rad. The vertical lines show the intensities of the discrete n components of the real spectrum. The light gray shade shows the Doppler spectrum obtained from the vibration velocity distribution, with a continuous variable on the horizontal axis $n=(\nu-\nu_0)/\nu_A$. Both spectra fall abruptly beyond $n=\pm 30.3$, which corresponds to the Doppler shift associated with the maximum velocity. (b) The dashed line shows the values n_1 as a function of Φ, where n_1 is the value of n giving the maximum intensity in the discrete spectrum; the solid line shows n_2, where n_2 is the value of n for which the intensity is half the maximum, which gives a very good approximation of Φ. (c) The dashed and solid curves, respectively, show $n_1-\Phi$ and $n_2-\Phi$ as a function of Φ.

Figures 1(b) and 1(c) give more detail on this sharp variation. For each value of Φ we calculate the value $n_1(\Phi)$ of n that, in Eq. (4), gives the maximum intensity. To avoid the quantization noise induced by discrete variables, the calculation is made with Bessel functions of fractional order, but of course only integer values of n are relevant to the experiment. It is known [8] that $n_1(\Phi)\simeq\Phi$, within a correction of order $\Phi^{1/3}$; the dashed curves show $n_1(\Phi)$ [Fig. 1(b)] and the difference $n_1(\Phi)-\Phi$ [Fig. 1(c)]. To determine more precisely the location of the abrupt drop from maximum to zero, we calculate the n value $n_2(\Phi)$ for which the intensity is half the maximum. The $n_2(\Phi)$ and the difference $n_2(\Phi)-\Phi$ are shown by the solid curves in Figs. 1(b) and 1(c), respectively. Clearly, n_2 gives an accurate evaluation of Φ.

The experimental setup is the same as described in [4]. As in [4], we have chosen a clarinet reed as the vibrating object to experimentally demonstrate the method. The reed, vibrating on its first flexural resonance mode at frequency $\nu_A\sim 2100$ Hz, is illuminated at $\lambda=650$ nm by a laser field E_I at frequency ν_0. The CCD camera (frame frequency $\nu_{\mathrm{CCD}}=10$ Hz) records the interference pattern (the hologram) between the scattered light and the local oscillator beam (field E_{LO}, frequency ν_{LO}). Two acousto-optic modulators (Bragg cells) with frequencies ν_{AOM1} and ν_{AOM2} are used to adjust the frequencies $\nu_0=\nu_L+\nu_{\mathrm{AOM2}}$ and $\nu_{\mathrm{LO}}=\nu_L+\nu_{\mathrm{AOM1}}$; an arbitrary sideband n can then be selected by adjusting these frequencies. A four-phase detection of sideband n is obtained by adjusting them to fulfill the relation

$$\nu_0+n\nu_A-\nu_{\mathrm{LO}}(n)=\nu_{\mathrm{CCD}}/4. \tag{5}$$

We record a sequence of consecutive CCD images $I_0,I_1,\ldots I_{M-1}$, where M is a multiple of 4. The complex hologram H in the plane of the CCD is then

$$H=\sum_{m=0}^{M-1} j^m I_m. \tag{6}$$

From H, the images are reconstructed as in [4] by the standard convolution method [2], which provides the map of the complex field $E(x,y,n)$ in the plane of the object. By successively adjusting the frequency $\nu_{\mathrm{LO}}(n)$ of the local oscillator to appropriate values, we then record the intensity images $|E(x,y,n)|^2$ of the sidebands as a function of x and y and n. We then obtain a cube of data with three axes x, y, and n, where x and y are expressed in units of pixels of the reconstructed image of the reed. Figure 2 shows the images obtained for for $n=0,20,\ldots 120$ that correspond to cuts of the cube along the x,y planes. The right part of the reed ($x>800$) is clamped on the mouthpiece. The images illustrate how, when n increases, the fringes move toward regions with larger amplitudes of vibrations: no signal is obtained in regions where $\Phi=4\pi z_{\max}/\lambda\leqslant n$. This well-known property of Bessel functions allows one to get a marker on the object, signaling regions where the amplitude corresponds to $\Phi\simeq 120$ rad. Figure 3(a) displays a cut of the cube of data along the x,n horizontal plane $y=750$ (horizontal white dashed line in Fig. 2). The envelope of the nonzero (nonblack) part of the image provides a measurement of the amplitude of vibration in units of $\lambda/4\pi$. We actually obtain a direct visualization of the shape of the reed at maximal elongation, from the right part clamped on the mouthpiece to the tip on the left. The maximum amplitude correspond to $\Phi\simeq 20, 40, 60,\ldots 120$ rad. Figure 3(b) displays a transverse cut along the y,n vertical $x=249$ plane (vertical white dashed line in Fig.

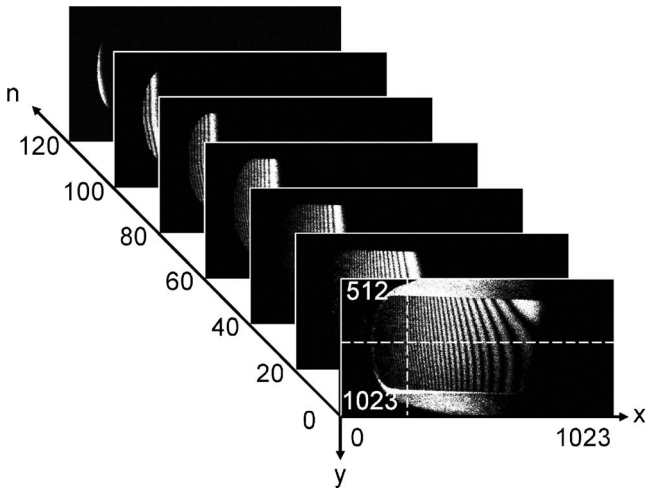

Fig. 2. Cube of data obtained from the reconstructed holographic images of a vibrating clarinet reed; sideband images with $n=0,20,40\ldots 120$ are shown in arbitrary linear scale. By choosing n, one moves the border of the illuminated region on the object, obtaining a local marker of the amplitude of vibration. The white dashed lines correspond to $x=249$ and $y=750$, i.e., to the point chosen for Fig. 3.

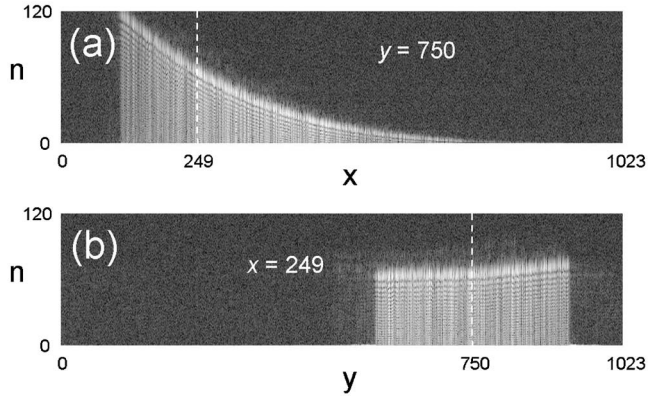

Fig. 3. Images corresponding to cuts of 3D data of the reconstructed images along the planes $y=750$ (a) and $x=249$ (b). (a) Deformation of the object along its axis. (b) Transverse cut with a slight vibration asymmetry. A logarithmic intensity scale is used.

2); a slight asymmetry of the reed vibration is clearly visible.

Figures 2 and 3 have been obtained by exciting the reed at the resonance frequency $\nu_A=2123$ Hz and at moderate excitation level. The consistency of amplitude measurements obtained in this way with those obtained by fringe counting is illustrated in Fig. 3 of [4]. We have also used higher excitation amplitudes, about 10 times larger (the frequency of reed resonance is then shifted to $\nu_A=2020$ Hz). Figure 4(a) shows the images obtained for $n=330$: the fringes are now completely unresolved, but the transition from zero to nonzero intensity remains very clear. With a single hologram, and without fringe counting, one obtains a clear marker of the line where $\Phi(x,y)=330$ rad.

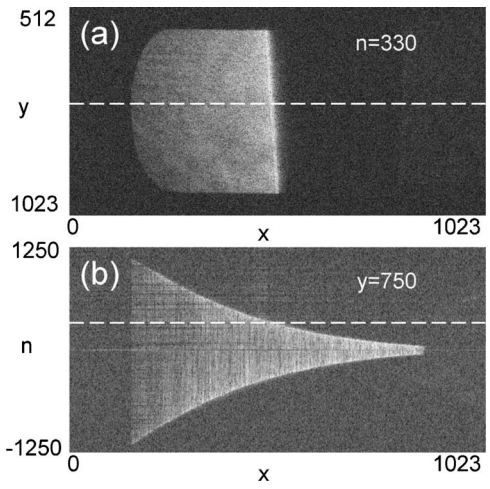

Fig. 4. (a) Image reconstructed with sideband $n=330$, with a large amplitude of vibration. (b) Equivalent of Fig. 3(a), but with positive and negative n values quantized by steps $\Delta n=10$; one measures a maximum vibration amplitude of $z_{\max}\simeq 60$ μm. An enlarged view of the $n\geqslant 0$ part of the image is provided in supplementary material (Media 1). A logarithmic intensity scale is used.

Figure 4(b) shows the equivalent of Fig. 3(a) but with a higher excitation level, and this time for positive and negative values of n; data range up to about $|n|\simeq 1140$, corresponding to $z_{\max}\simeq 58.4$ μm. Since the vibration amplitude is much larger than λ, the continuous approximation for n is valid, and the images of Fig. 3 can be reinterpreted in terms of the classical Doppler effect: if the signal intensity $I_n(x,y)$ at frequency $\nu_0+n\nu_A$ is nonzero, at some time t of the periodic motion the Doppler shift $\nu_0+2v(x,y,t)/c$ is equal to $n\nu_A$ (v and c are the reed and light velocities). The accuracy of the measurement of the amplitude corresponds to about one step: $\Delta n=10$, i.e., to 0.5 μm [see Fig. 4 (Media 1)]. A fine analysis of the 3D data shows a slight asymmetry between the positive and the negative n values. In Fig. 4(b), for example, the maximum value for $|n|$ is about 1160 for $n>0$ and 1120 for $n<0$. This means that the motion of the reed is not perfectly sinusoidal and that maximum velocities (i.e., maximum Doppler shifts) are slightly different for the up and down motion of the reed. A more detailed study of the modification of the spectrum due to the superposition of several harmonic motions can be done but falls beyond the scope of this Letter.

In conclusion, taking advantage of the frequency (or the sideband order n) of the light scattered by a vibrating object adds a new dimension to digital holography. Each pixel of the image then provides information that is completely independent of the others, which results in redundancy and robustness of the measurements. Looking at the edges of the spectrum provides an accurate determination of the vibration amplitude and avoids a cumbersome analysis of the entire data cube, giving easy access to measurements of large amplitudes of oscillation. Our method could be combined with other techniques, such as phase modulation of the reference beam [9,10], to yield information on the phase of the mechanical vibration without losing the robustness of the measurement.

References

1. R. Powell and K. Stetson, J. Opt. Soc. Am. **55**, 1593 (1965).
2. U. Schnars and W. Jüptner, Appl. Opt. **33**, 179 (1994).
3. P. Picart, J. Leval, D. Mounier, and S. Gougeon, Opt. Lett. **28**, 1900 (2003).
4. F. Joud, F. Laloë, M. Atlan, J. Hare, and M. Gross, Opt. Express **17**, 2774 (2009).
5. C. Aleksoff, Appl. Opt. **10**, 1329 (1971).
6. M. Atlan and M. Gross, Rev. Sci. Instrum. **77**, 116103 (2006).
7. M. Atlan, M. Gross, B. Forget, T. Vitalis, A. Rancillac, and A. Dunn, Opt. Lett. **31**, 2762 (2006).
8. M. Abramowitz and I. Stegun, *Handbook of Mathematical Functions with Formulas, Graphs, and Mathematical Table* (Courier Dover, 1965).
9. O. Lokberg, J. Acoust. Soc. Am. **96**, 2244 (1994).
10. F. Zhang, J. Valera, I. Yamaguchi, M. Yokota, and G. Mills, Opt. Rev. **11**, 297 (2004).